Seventh International Conference on CFD in the Minerals and Process Industries
CSIRO, Melbourne, Australia
9-11 December 2009

EXTERNAL CHARACTERISTICS OF SPRAY ATOMISATION FROM A NASAL SPRAY DEVICE

Man Chiu FUNG[1], Kiao INTHAVONG[1], William YANG[2] and Jiyuan TU[1]

[1] School of Aerospace, Mechanical and Manufacturing Engineering, RMIT University, AUSTRALIA
[2] CSIRO Minerals, Clayton, Victoria 3169, AUSTRALIA

ABSTRACT

Atomisation of liquids is a complicated process. It is common in many industries such as automotive, manufacturing (spray drying) and mineral processing. These industries often use high-pressure spray devices and its studies are common in the literature. However, in the pharmaceutical industry atomisation occurs under low pressure and studies in the literature are not as common. Spray formation was simulated in Ansys CFX under a Lagrangian model. The primary breakup Blob model is used to handle atomisation of the liquid while the secondary breakup TAB and ETAB models are evaluated for the subsequent breakup of the atomised droplets. Two-way coupling was applied in order to simulate the interaction between initial ambient gas and the liquid droplets. It was found that the spray half cone angle was unexpectedly large at early spray development in the simulation, but the calculated results matched better with the experimental results in the later stages of spray development. The study also demonstrated that the ETAB model had a better prediction of axial penetration and radial range in the 6 bar high pressure injection case over the TAB model. However the TAB model did perform better under a lower injection pressure case.

NOMENCLATURE

A Area
C_D Drag coefficient
D Diameter
K_{br} Breakup Constant
m Mass
M_p Momentum
$\dot{m}$ Mass flow rate
$n(t)$ Number of particles
On Ohnesorge number
r Radius
Re Reynolds number
t_{bu} Breakup time
U Velocity
V_N Normal velocity
V_{slip} Slip velocity
We Weber number
x Displacement
y Droplet dimensionless deformation
$\dot{y}$ Droplet dimensionless deformation rate
$\ddot{y}$ Acceleration of droplet dimensionless deformation

α void fraction
μ dynamic viscosity
ρ density
σ surface tension
υ kinematic viscosity
υ_T eddy viscosity
ω frequency of wave motion

subscripts

d dispersed phase
g gaseous phase
m mixture
p particle

INTRODUCTION

Spray is a common method for spreading liquids in various situations. Characterisation of sprays and their performance has been reported extensively in manufacturing, and automotive industries. Spray atomisation is also prominent in the pharmaceutical industry through drug delivery such as nasal sprays but its studies are lacking. Nasal drug delivery provides an alternative to traditional delivery methods such as the oral drug route or intravenous, since digestion leads to a breakdown of the drug formulation by the gastric acid inside stomach while intravenous leads to non-compliance by patients due to the pain associated with injection. The nasal turbinates that are lined with highly vascularised mucosa provides a pathway for drugs to enter the bloodstream. It has potential to deliver a systemic response at high levels of therapeutic efficacy of the drug composition. Because of these characteristics it is hypothesised that if drug formulation can be deposited in the turbinated region, this delivery method will open up more opportunities to tackle systemic health problems such as cancers, lung diseases, sinus infections (Kimbell et al. 2007). Therefore, studies of local particle deposition are important for effective drug delivery via the nasal cavity.

Evaluating the performance of nasal sprays has mainly been based upon in-vitro methodologies set by the US Food and Drug Administration (FDA). These tests include emitted dose, droplet or particle size distribution, spray pattern, and plume geometry which aim to evaluate the bioavailability and bioequivalence of the nasal spray device. In-vivo methods to determine deposition patterns are performed through radionuclide imaging methods such as 2D gamma scintigraphy imaging (Suman et al. 2002) or 3D positron emission tomography (PET). Alternative methods also include direct spray particle deposition experiments within a nasal cavity cast (Cheng et al. 2001) and numerical simulations by Computational Fluid Dynamics (CFD) (Inthavong et al. 2006).

Suman et al. (2002) evaluated in-vitro testing methodologies as set by the FDA guidelines on two aqueous spray pumps as a surrogate means for particle deposition. The impact of actuation force, actuation distance, and rheological properties of the drug formulation on spray pattern, particle size distribution, plume area, and ovality was performed by Dayal et al. (2004) Characterisation of four nasal sprays was performed by Cheng et al. (2001) using laser diffraction to obtain the particle size distribution and still photographic images for the spray angle. Guo and Doub (2006) investigated the influence of actuation parameters, such as stroke length, actuation velocity, and actuation acceleration, to ascertain how they affect nasal spray characteristics. These experiments were performed using commercially available measuring instruments designed specifically for nasal spray actuation.

The atomisation and spray formation processes of a nasal spray are relatively small scale and high speed in nature due to the drug formulation being atomised through small diameter orifices, which makes it difficult to study experimentally. An alternative method to evaluate the performance of nasal sprays is through CFD. There have been a small number of research papers that have reported the effects of spray characteristics on particle deposition by CFD. These include: spray cone angle, initial particle velocity, and insertion angle (Inthavong et al. 2006); particle release location, insertion angle, spray velocities, and spray cone angle (Kimbell et al. 2007). In both studies particle release points were defined at the nasal spray nozzle tip and the simulation was under steady state. The initial boundary conditions imposed on the atomised particles were set by defining vector directions for the spray cone angles, and a linear velocity. In this paper, a CFD simulation is performed to visualise the external characteristics of the spray formation. Experimental images were obtained through high speed photography, in order to validate the models and investigate external spray characteristics such as the spray penetration, and atomisation in the near nozzle region. To complement the experimental measurements, a CFD simulation is performed to provide more details.

EXPERIMENT

In experiment, the actuator was set to press the nasal spray when it was contracting. The time between extension and contraction is about 4 seconds. Therefore, totally 8 seconds is allowed for the settling of water droplets. Trial photographing was performed to ensure that the time was sufficient for droplet settling. The nasal spray device was pressed for 4 times in each experiment, so it was easier for the photographer to choose the best timing to capture the spray development. The experimental actuating station is controlled by a programmable logic control (PLC) unit which was designed for repeated experimental measurements. A pneumatic actuator was attached to it and provided pressure on the nasal spray device (Figure 1). The actuator's motion is shown in the step diagram (Figure 2). 0 represents the contraction location while 1 represents the extension location. Both contraction and extension lasts for 4 seconds.

The external characteristics of the spray were recorded by a high speed camera. The camera's exposure and shutter speed was adjusted and the experiment was repeated to ensuring quality of results. Image capturing was proformed only in one out of the four cycles of spraying action. Image processing was handled by Photoshop by determining the pixel distances and scaling it to the correct measurement(Laryea & No 2004).

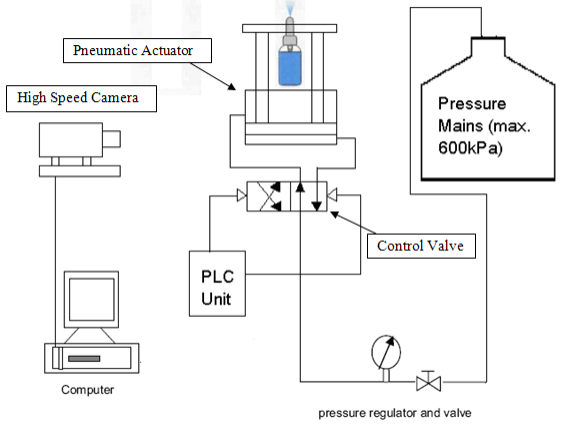

Figure 1: Test Station

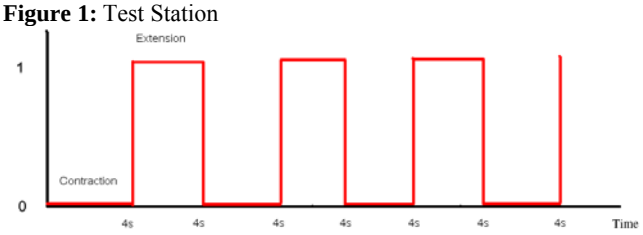

Figure 2 Step diagram of the actuator's motion

NUMERICAL MODEL

Fluid Modelling

The standard *k-ε* turbulence is applied for the numerical calculation of turbulent two-phase flow. The governing equations for the fluid phase are given as:

Continuity

$$\frac{\partial \alpha_g}{\partial t} + \frac{\partial}{\partial x}(\alpha_g u_i^g) = 0 \qquad (1)$$

Momentum equation

$$\frac{\partial \alpha_g u_i^g}{\partial t} + u_j^g \frac{\partial \alpha_g u_i^g}{\partial x_j} = -\frac{\alpha_g}{\rho_g}\frac{\partial p_g}{\partial x_i} + \frac{\partial}{\partial x_j}[\alpha_g(\upsilon + \upsilon_T)(\frac{\partial u_i^g}{\partial x_j} + \frac{\partial u_j^g}{\partial x_i})] \qquad (2)$$
$$+ \frac{1}{\alpha_g \rho_g} M_p$$

Turbulent Kinetic Energy, (*k* equation)

$$\frac{\partial(\rho k)}{\partial t} + \nabla \bullet (\rho U k) = \nabla \bullet \left[\left(\mu + \frac{\mu_t}{\sigma_g}\right)\nabla k\right] + P_k - \rho\varepsilon \qquad (3)$$

Turbulence Dissipation Rate Equation, (*ε* equation)

$$\frac{\partial(\rho\varepsilon)}{\partial t} + \nabla \bullet (\rho U \varepsilon) = \nabla \bullet \left[\left(\mu + \frac{\mu_t}{\sigma_g}\right)\nabla \varepsilon\right] + \frac{\varepsilon}{k}(C_{\varepsilon 1} P_k - C_{\varepsilon 2}\rho\varepsilon) \qquad (4)$$

Particle Trajectory modelling

The particles (disperse phase) are modelled with the Lagrangian approach. Trajectory of liquid droplets is tracked using a two-way coupling with the fluid phase. The scheme is performed by integrating the force balance equations for individual particles (Shi & Kleinstreuer 2007)

$$\frac{dx_p}{dt} = u_p \tag{5}$$

$$m_p \frac{du_p}{dt} = \frac{1}{8}\pi\rho_p d_p^2 C_D (u_g - u_p)\left|u_g - u_p\right| \tag{6}$$

The interphase drag term is determined by Ishii-Zuber (1979) drag model

$$C_D = \frac{24}{\mathrm{Re}_m}\left(1 + 0.15\,\mathrm{Re}_m^{0.687}\right) \text{ for Re < 1000} \tag{7}$$

when the droplets are in the viscous regime, the drag coefficient is identical to the Schiller Naumann correlation (Clift, Grace & Weber 1978)and the shape of droplet is assumed to be spherical.

Re_m is the mixture Reynolds number which is defined as

$$\mathrm{Re}_m = \frac{\rho_m d_p \left|u_p - u_g\right|}{\mu_m} \tag{8}$$

In the distorted fluid particle regime, there is increased drag on fluid particles, due to the wake characteristics of turbulent eddies and particle motions. The Drag coefficient becomes:

$$C_d = \frac{4}{3} r_p \sqrt{\frac{g\Delta\rho}{\sigma}} \left\{ \frac{1 + 17.67\left[f(\alpha_d)\right]^{6/7}}{18.67 f(\alpha_d)} \right\}^2 \tag{9}$$

Where $f(\alpha_d) = (1-\alpha_d)^{1/2}\mu_g / \mu_m$

An additional correction formula is used to determine the dynamic drag coefficient of deformed droplets (Liu, Mather & Reitz 1993)

$$C_{D,droplet} = C_d(1 + 2.63y) \quad 0<y<1 \tag{10}$$

where y= 1 when the particle is maximally distorted

Primary Breakup

Primary Breakup model used in this study is BLOB method. It is the simplest approach which ignores the detailed description of the atomization process within the primary breakup zone of spray. The nozzle's size is used as the initial drop diameter (Eqn. 11).

$$D_p = D_{nozzle} \tag{11}$$

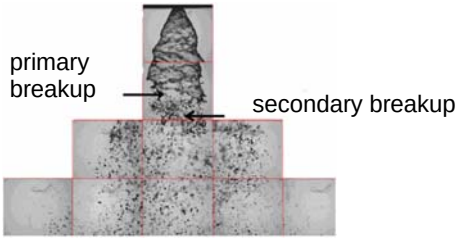

Figure 3 Primary breakup and secondary breakup region

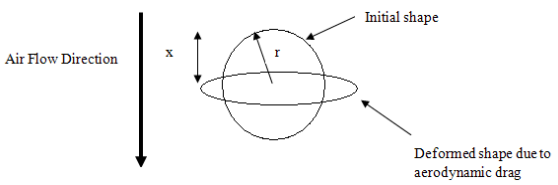

Figure 4: Droplet deformation in airflow (by the TAB model)

By conservation of mass, the droplet injection velocity is determined by:

$$U_{p,initial}(t) = \frac{\dot{m}_{nozzle}(t)}{A_{nozzle}\rho_p} \tag{12}$$

Where A_{nozzle} is the nozzle cross section area and $\dot{m}_{nozzle}$ is the mass flow rate through nozzle.

Droplets with the size identical to nozzle diameters are injected and are subjected to aerodynamic induced secondary breakup.

Secondary Breakup

After primary breakup, the particles are exposed to the flow field where a shear layer occurs between the moving droplets and the stagnant air. This causes secondary breakup of the droplets into smaller droplets (Figure 3). This process is simulated by the Taylor Analogy Breakup (TAB) and Enhanced Taylor Analogy Breakup (ETAB) models for comparison in this study. The TAB model considers the droplet distortion and oscillation based on the analogy of, a spring-mass system. The droplet deformation is expressed by the formula y=2(x/r), where x is the deviation of droplet equator (Figure 4). Liquid viscosity acts as damping force and the surface tension as a restoring force (O'Rourke & Amsden 1987)

$$\ddot{y} = \frac{2\rho_g V_{slip}^2}{3\rho_g r^2} - \frac{8\sigma}{\rho_P r^2} y - \frac{5\mu_P}{\rho_P r^2}\dot{y} \tag{13}$$

At the time of breakup the equator of parent droplet moves at a velocity of $V_N = \frac{1}{2} r\dot{y}$. The spray angle can be determined by following formula:

$$\tan\frac{\theta}{2} = \frac{V_N}{V_{slip}} \tag{14}$$

After breakup of the parent droplet, the deformation parameters of the subsequent child droplets are set to $y(0) = \dot{y}(0) = 0$.

For the ETAB model, which is a modified version of the TAB model the rate of child droplet formation is proportional to the number of child droplets (Tanner 1997):

$$\frac{dn(t)}{dt} = 3K_{br}n(t) \tag{15}$$

The normal velocity V_N is denoted by the equation

$$V_N = A\dot{x} \tag{16}$$

Where A is a constant determined from an energy balance:

$$A^2 = 3\left[1 - \frac{r_{P,Parent}}{r_{P,Child}} + 5C_D We/72\right]\frac{\omega^2}{\dot{y}^2} \tag{17}$$

It has been found that the TAB model largely underestimates the breakup times which will greatly affect the penetration depth and local droplet size distribution (Tanner 1997). In the ETAB model, this limitation is overcome by setting the initial rate of drop deformation to the largest negative root while keeping the initial droplet deformation to be:

$$\dot{y}(0) = \left[1 - We_C\left(1 - \cos\omega t_{bu}\right)\right]\frac{\omega}{\sin\omega t_{bu}} \qquad (18)$$

Computational Setup

The volume is meshed with hexahedral elements, with O-grid at both ends, in order to get finer mesh for the injection path. Number of elements is about 82800 for preliminary analysis. The final mesh topology was determined by grid sensitivity test. The test was done by comparing the spray penetration. It was found that the 753519 elements mesh is sufficient, since the difference in penetration depth of models of finer mesh is not significant. The injection hole diameter is about 0.295mm. The boundary conditions are shown in Figure 5 and Table 1. Ten particles were injected every time step (0.05ms). The simulation is in transient mode with the first 10ms data extracted and compare with experimental data.

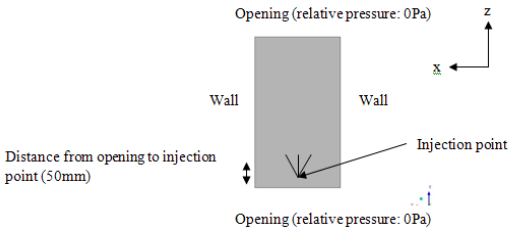

Figure 5: Boundary conditions

Table 1: Overview of data used in computations

	Case A (6bar)	Case B (2bar)
Mass Flow Rate (g/s)	1.42	0.42
Initial Cone Angle (deg)	22.62	16.64
Properties of Liquid (water)		
Density (kgm^-3)	997	
Reference Temperature (Celsius)	25	
Dynamic Viscosity (kgm^-1K^-1)	0.0008899	
Surface Tension Coefficient (dynecm^-1)	72	
Properties of gas (Air)		
Density (kgm^-3)	1.185	
Reference Temperature (Celcius)	25	
Dynamic Viscosity (kgm^-1K^-1)	1.83E-05	

Numerical schemes

Commercial finite-volume based program ANSYS CFX V11 was used in the research. The advection scheme used in this study is first order upwind scheme for accelerating the convergence. The second order scheme was not used, because it was found that k-ε turbulence model occasionally encountered convergence problem if using second order scheme in fully-coupled turbulent fluid-particle simulations (Shi & Kleinstreuer 2007). For the transient method, second-order backward Euler method was used.

RESULTS AND DISCUSSION

Comparison of Spray Half Cone Angle

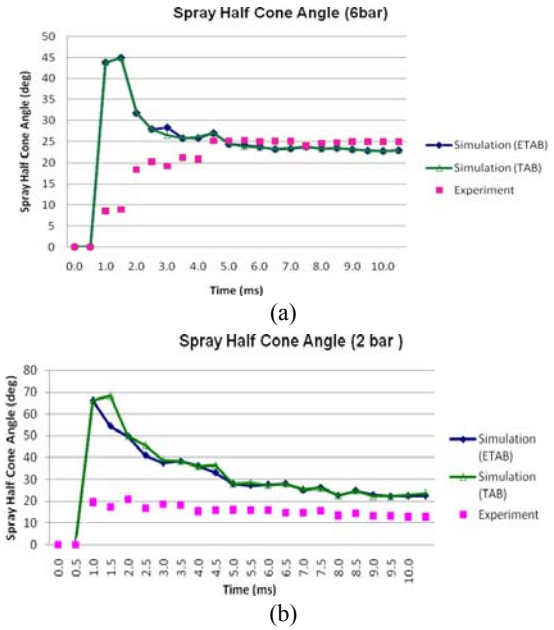

Figure 6 Comparison of Spray Half Cone Angle for (a) 6bar and (b) 2bar injection pressure.

The spray cone angle development of the TAB and ETAB models in the first 10ms is compared at two different injection pressures (Figure 6). Generally, the simulation results match experimental result well in later stages (t=4-10ms) for the 6 bar case, where the maximum difference is approximately 2 degrees. However, in the first 2 ms, there are some differences in the spray cone angle development. It is because of the BLOB model's assumption. In both cases, the jet breakup process is ignored, due to the application of BLOB model. The secondary breakup immediately takes place, because spherical droplets with uniform size are injected to the volume, instead of obtaining water droplets from the atomisation of water jet. The short axial distance of droplet causes the large initial spray cone angle (Figure 7). The ignoring of the presence of water jet causes the cone angle to be quite large even the radial range is very short. However, in later time steps, the spray droplet travelled to a longer distance, the spray angles matched with the simulation result. For the 2 bar case, the huge difference between simulation and experimental result is due to the incomplete atomisation under low injection pressure.

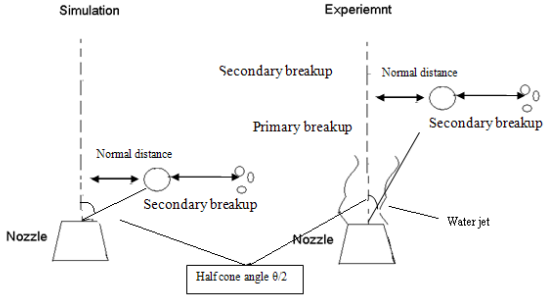

Figure 7 Determination of half cone angle θ/2

Comparison of Axial Penetration

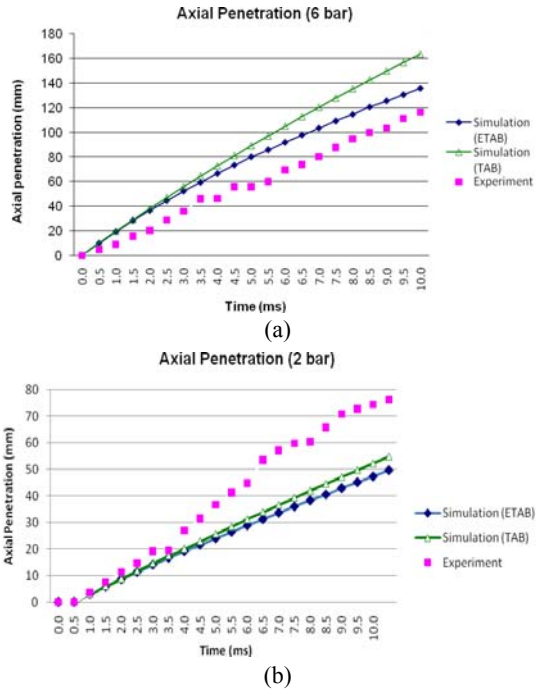

Figure 8 Comparison of Axial Penetration for (a) 6bar and (b) 2bar injection pressure.

Normally, the TAB model gives a deeper axial penetration, because the TAB model simulates only secondary breakup. The jet breakup is not simulated, but assumes the initial spray condition at the nozzle exit. The well atomized spray induces a stronger air flow which leads to the deeper axial penetration at the initial stage. The ETAB model was originally developed for high pressure applications, where its modification from the TAB model was to prolong the under predicted breakup time in high pressure cases. This is achieved by assuming the droplet deformation rate to be initially the same as an elliptical droplet. When the droplets travel in the opposite direction to the air flow, it becomes deformed to an elliptic disc shape before breakup.

Comparisons of the axial penetration for the secondary breakup models showed that the ETAB model gave a superior result for the higher injection pressure case while the TAB model matched the experimental result slightly better in the low injection pressure case. In the high injection pressure case, the ETAB model performed better, because the droplets were more likely to be distorted as blimp like shape under high speed (Tanner 1997) (Figure 9). Therefore, the breakup time and particle velocity calculated by ETAB model is more realistic.

Nonetheless, in the lower injection pressure case, the pressure is not sufficient to produce a blimp like initial shape, but rather the deformation is more spherical, which is closer to the assumption of the TAB model. Additionally droplet agglomeration in the near nozzle region was neglected which may have contributed to the underestimated axial penetration.

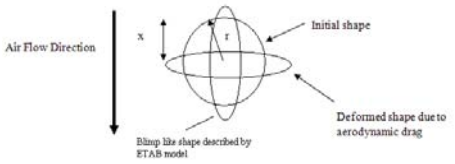

Figure 9 Blimp like shape described by ETAB model

Comparison of Radial Range

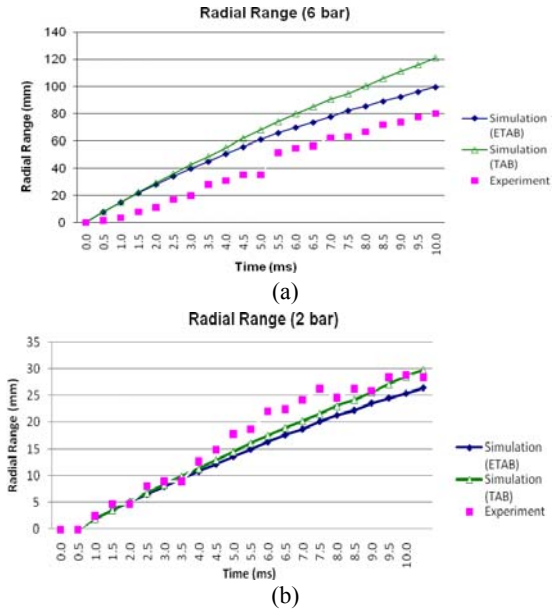

Figure 10 Comparison of Radial Penetration for (a) 6bar and (b) 2bar injection pressure.

Radial Range is the measurement of travel distance of droplets in normal direction after breakup. Radial dispersion is related to the droplet size and the rate of drop deformation $\dot{y}$. It can be determined by $V_N=A\,\dot{x}$. The constant A is determined through Eqn. 16 and 17. In the standard TAB model, the parent drop deformation velocity goes into the normal velocity component of the child product droplets is usually larger than that in ETAB model. It was revealed by the comparison of a typical droplet in previous research (Tanner 1997). This leads to the TAB model always exhibiting a larger radial dispersion. The spray cone angle is closely related to the radial dispersion, since both of them are dependent on the normal velocity V_N. However, they do not have an identical trend in simulation. The reason is the absence of the simulation of primary breakup which was stated in previous section of the comparison of spray cone angle..

Comparison of the radial penetration shows similar performance of the two secondary breakup models which is similar to that of the axial penetration. The ETAB model for the radial dispersion performs better in the high injection pressure case while the TAB model works better for the low injection pressure case.

The images of experiments and simulations are illustrated in Figure 11 for comparison. The simulation results herein are calculated by the ETAB model only. ETAB model results were chosen for visualisation comparison for two reasons. Firstly, ETAB model gives better prediction in the high injection pressure case. Secondly, the prediction for low injection pressure case showed minimal difference with the TAB model.

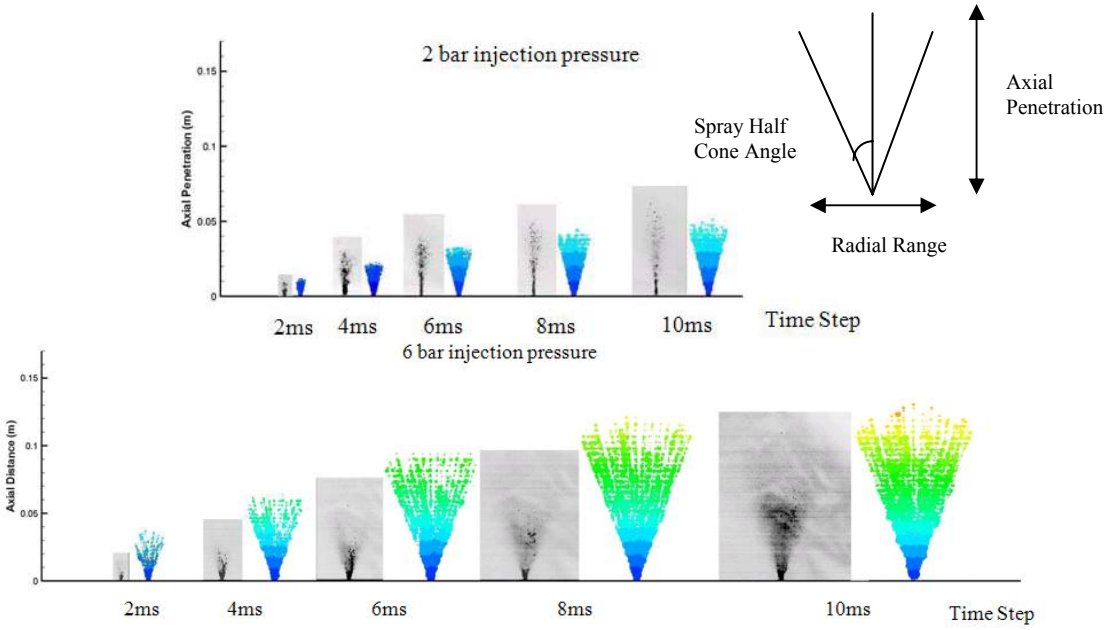

Figure 11: Comparison of axial penetration for different injection pressures

CONCLUSION

This study demonstrates the external characteristics of spray atomisation through a CFD simulation and experimental measurement. In the CFD simulation, the TAB and ETAB model was compared. It was found that the spray half cone angle was unexpectedly large in early spray development in the simulation, but the calculated results matched better with the experimental results in the later stages of spray development. The study also demonstrated that the ETAB model had a better prediction of axial penetration and radial range in the 6 bar high pressure injection case over the TAB model. However the TAB model did perform better under a lower injection pressure case. For the radial range, the trend of the performance of TAB and ETAB models were similar to that of the axial penetration. The ETAB model worked better in the high injection pressure case and the TAB model worked better in the low injection pressure case.

ACKNOWLEDGEMENT

The financial support from RMIT scholarship is gratefully acknowledged.

REFERENCES

CHENG, Y. S., HOLMES, T. D., GAO, J., GUILMETTE, R. A., LI, S., SURAKITBANHARN, Y. & ROWLINGS, C. (2001) Characterization of nasal spray pumps and deposition pattern in a replica of the human nasal airway. *J. Aerosol Med.,* 14**,** 267-280.

CLIFT, R., GRACE, J. R. & WEBER, M. E. (1978) *Bubbles, drops, and particles,* New York, Academic Press.

DAYAL, P., SHAIK, M. S. & SINGH, M. (2004) Evaluation of different parameters that affect droplet-size distribution from nasal sprays using Malvern Spraytec. *J. Phar. Sci.,* 93**,** 1725-1742.

GUO, C. & DOUB, W. H. (2006) The influence of actuation parameters on in vitro testing of nasal spray products. *Journal of Pharmaceutical Sciences,* 95**,** 2029-2040.

INTHAVONG, K., TIAN, Z. F., LI, H. F., TU, J. Y., YANG, W., XUE, C. L. & LI, C. G. (2006) A numerical study of spray particle deposition in a human nasal cavity. *Aerosol Science Technology,* 40.

ISHII, M. & ZUBER, N. (1979) DRAG COEFFICIENT AND RELATIVE VELOCITY IN BUBBLY, DROPLET OR PARTICULATE FLOWS. *AIChE Journal,* 25**,** 843-855.

KIMBELL, J. S., SEGAL, R. A., ASGHARIAN, B., WONG, B. A., SCHROETER, J. D., SOUTHALL, J. P., DICKENS, C. J., BRACE, G. & MILLER, F. J. (2007) Characterization of deposition from nasal spray devices using a computational fluid dynamics model of the human nasal passages. *J. Aeros. Med.,* 20**,** 59-74.

LARYEA, G. N. & NO, S. Y. (2004) Spray angle and breakup length of charge-injected electrostatic pressure-swirl nozzle. *Journal of Electrostatics,* 60**,** 37-47.

LIU, B., MATHER, D. & REITZ, R. D. (1993) Effects of Drop Drag and Breakup on Fuel Sprays. *SAE Technical Paper*

O'ROURKE, P. J. & AMSDEN, A. A. (1987) The TAB Method for Numerical Calculation of Spray Droplet Breakup. *SAE Technical Paper,* 872089.

SHI, H. & KLEINSTREUER, C. (2007) Simulation and Analysis of High-Speed Droplet Spray Dynamics. *Journal of Fluids Engineering,* 129**,** 621-633.

SUMAN, J. D., LAUBE, B. L., LIN, T. C., BROUET, G. & DALBY, R. (2002) Validity of in vitro tests on aqueous spray pumps as surrogates for nasal deposition. *Pharma. Res.,* 19**,** 1-6.

TANNER, F. X. (1997) Liquid Jet Atomization and Droplet Breakup Modelling of Non-Evaporating Diesel Fuel Sprays. *SAE Technical Paper,* 970050.

